Global partial density of states: Statistics and localization length in quasi-one-dimensional disordered wires

J. Ruiz
Departamento de Física, Universidad de Murcia, Apartado 4021, E-30080 Murcia, Spain

E. Jódar
Departamento de Física Aplicada, Universidad Politécnica de Cartagena, E-30202 Cartagena, Murcia, Spain

V. Gasparian
Department of Physics, California State University, Bakersfield, California 93311, USA
(Received 19 October 2006; revised manuscript received 23 March 2007; published 26 June 2007)

We study numerically the behavior of the distributions functions for diagonal and off-diagonal elements of the global partial density of states (DOS) in quasi-one-dimensional (Q1D) disordered wires as a function of disorder parameter from metal to insulator. We consider two different models for disordered Q1D wire: a set of two-dimensional N scatterers of δ potentials with arbitrary signs and strengths placed randomly and a tight-binding Hamiltonian with several modes M and on-site disorder. We show that the variances of global partial DOS in the metal to insulator crossover regime are crossing. The critical value of disorder w_c, where we have crossover for given numbers of N scatterers and for modes M, can be used for calculating a localization length in Q1D systems. The matrix elements of Green's function of Dyson's equation in Q1D wires for the two models are calculated analytically. It is shown that the Q1D problem can be mapped to the 1D problem and that the poles of the Green's function matrix elements, as well as the scattering matrix elements, are a determinant of rank $N \times N$, where N is the number of scatterers. It is shown that the determinant can be used to calculate the spectrum of an electron in the disordered Q1D wire, the DOS, the scattering matrix elements, etc., without determining the exact electron wave function.

DOI: 10.1103/PhysRevB.75.235123 PACS number(s): 73.23.−b, 72.10.Bg, 72.15.Rn, 05.45.−a

I. INTRODUCTION

Calculating the density of states (DOS) allows us to obtain many properties of the system under consideration, such as charging effects, electrical conduction phenomena, tunneling spectroscopy, or thermodynamic properties. Furthermore, the decomposition of DOS in the partial density of states (PDOS) and global PDOS plays an important role in dynamic and nonlinear transport in mesoscopic conductors.[1–8] Particularly, the emissivity, which is the PDOS in configuration space for electrons emitted through arbitrary lead,[2,9,10] is always present in physical phenomena where quantum interference is important. The adiabatic quantum pump and its noise properties, the heat flow, etc., can be expressed in terms of a generalized parametric emissivity matrix $\nu[X]$ (see Ref. 8). The diagonal element $\nu_{\alpha\alpha}[X]$ of the emissivity matrix is the number of electrons entering or leaving the device in response to a small change $\delta U(x)$, such as distortion of the confining potential. The off-diagonal element $\nu_{\alpha\beta}[X]$ of the parametric emissivity matrix determines the correlation between the current in leads α and β due to variation of parameter X.[11]

Note that the elements of global PDOS are closely related to characteristic times of the scattering process and consequently to the absolute square of the scattering states. Particularly, in one-dimensional (1D) systems, $\nu_{\alpha\beta}$ and $\nu_{\alpha\alpha}$ are related to the Larmor transmitted time τ_T (or Wigner delay time) and to the reflected time τ_R which are, respectively, weighted by the transmission coefficient T (Refs. 5, 12, and 13) and reflection coefficient R. The Wigner delay time can be interpreted as a time delay in propagation of the peak of the wave packet due to scattering in comparison with a free wave packet propagation. The theory of weighted delay time for a waveguide in the diffusive regime, when the length L of the system exceeds the mean free path but is still less than the localization length ξ, is formulated in Refs. 14 and 15. They have shown that the weighted single-channel delay time is not a self-averaging quantity and that large mesoscopic fluctuations in delay time can be expected. These fluctuations, as we will see in Sec. IV, will affect the statistics of the diagonal and off-diagonal elements of the parametric emissivity matrix.

As was mentioned in Ref. 16, the emittance is in general not capacitancelike, i.e., the diagonal and the off-diagonal emittance elements are not positive and negative values, respectively. Whenever the transmission of carriers between the two contacts predominates the reflection, the associated emittance element changes sign and behaves inductancelike. This type of crossover behavior for the diagonal element of emittance $\nu_{\alpha\alpha}$ (taking into account the Coulomb interaction of electrons inside the sample) was found in Ref. 17, where the authors studied the distribution function (DF) of emittance. They found that in the range of weak disorder, when the system is still conductive, the DF is Gaussian-like. With increasing disorder of the system, the DF becomes non-Gaussian. In other words, the system shows inductivelike dynamic behavior when the system is almost transparent, and it behaves capacitivelike when we have complete reflection from the system.

The purpose of this paper is to study numerically the behavior of DFs of the diagonal elements $\nu_{\alpha\alpha}$ and off-diagonal

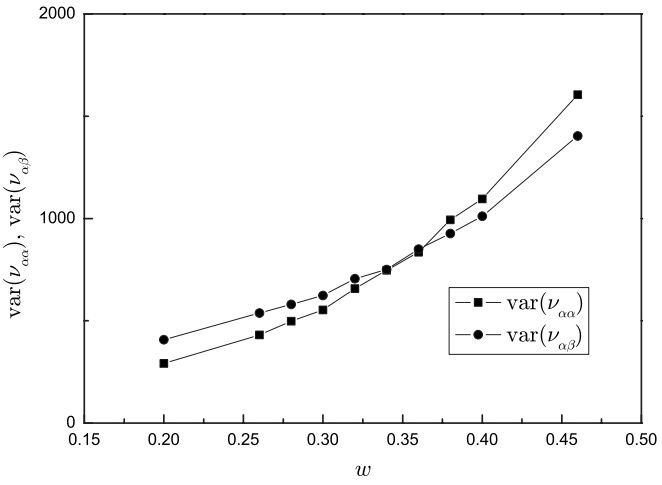

FIG. 1. Crossover between $\mathrm{var}(\nu_{\alpha\alpha})$ and $\mathrm{var}(\nu_{\alpha\beta})$ for sample of $L=400$ and $M=4$.

elements $\nu_{\alpha\beta}$ of global PDOS in the Q1D disordered wires, where not much is known about the behavior of the DF. We will be interested in the three different regimes of transport: metallic ($\xi \gg L$) (where ξ is the localization length and L is the typical size of the system), insulating ($\xi \ll L$), and crossover ($\xi \sim L$). Our results indicate that in the intermediate regime of transport between the metallic and insulating regimes, there exists a critical value of disorder w_c where we observe crossover between the variances $\mathrm{var}(\nu_{\alpha\alpha})$ and $\mathrm{var}(\nu_{\alpha\beta})$ (see Fig. 1). This critical w_c determines the localization length of the Q1D system for given length L and number of modes M. It turns out that in the metallic regime, the distribution function $P(\nu_{\alpha\beta})$ is Gaussian, which means that the first and second moments (i.e., the average $\langle \nu_{\alpha\beta} \rangle$ and the variance $\mathrm{var}(\nu_{\alpha\beta}) = \langle \nu_{\alpha\beta}^2 \rangle - \langle \nu_{\alpha\beta} \rangle^2$) are enough to describe the behavior of $P(\nu_{\alpha\beta})$. In the strong localization regime, the distribution of $\nu_{\alpha\beta}$ is log-normal, which means that $\ln \nu_{\alpha\beta}$ follows a Gaussian distribution. As regards the distribution function of $\nu_{\alpha\alpha}$, we can say that in the strong localization regime, it is characterized by an exponential tail, the values of $\nu_{\alpha\alpha}$ are positive, and the dynamic response of the system is capacitivelike.[16] In the metallic regime, the emittance has non-Gaussian-like behavior and some of the values of $\nu_{\alpha\alpha}$ are negative (inductivelike behavior).[17,18]

We will consider two models: a Q1D wire with the set of δ scattering potentials of the form

$$V(x,y) = \sum_{n=1}^{N} V_n \delta(x - x_n)\delta(y - y_n), \tag{1}$$

where V_n, x_n, and y_n are arbitrary parameters, and a Q1D lattice of size $L \times W$ ($L \gg W$, L is the length and W is the width of the system). The site energy can be chosen randomly. In both cases we have calculated the Green's functions of 1QD (Ref. 19) analytically and used them in our numerical calculations (see the Appendix).

The elements of global PDOS $\nu_{\alpha\beta}$, in the case of a tight-binding model, can be calculated in terms of the scattering matrix and the Green's function as well. To this end, we start from the Fisher-Lee relation[20,21] between the scattering matrix, which corresponds to the transmission between modes n and m and the Green's function:

$$s_{nm} = -\delta_{nm} + \imath\hbar\sqrt{v_n v_m}\sum_{i,j} \chi_n(r_{0_i}) G(r_{0_i}, r_{0_j}) \chi_m(r_{0_j}). \tag{2}$$

Here, $\chi_m(r_{0_j})$ is the transverse wave function corresponding to mode m at point r_{0_j} and $G(r_{0_i}, r_{0_j})$ is the Green's function (GF) for noncoinciding coordinates. v_m is the velocity associated with propagating mode m. By recalling that the density response and the current response of the scattering problem can be expressed in terms of the local PDOS to linear order in a perturbation, $\delta U(x)$:[1]

$$\frac{dn_{nm}(r)}{dE} \equiv -\frac{1}{4\pi\imath}\left[s_{nm}^* \frac{\delta s_{nm}}{\delta U(r)} - \frac{\delta s_{nm}^*}{\delta U(r)} s_{nm} \right], \tag{3}$$

and when Eq. (2) is inserted into Eq. (3), we get

$$\frac{dn_{nm}}{dE}(r) = -\frac{\hbar\sqrt{v_n v_m}}{4\pi}\sum_{i,j} [s_{mn}^* \chi_n(r_{0_i}) G(r_{0_i}, r) G(r, r_{0_j}) \chi_m(r_{0_j}) + \mathrm{H.c.}], \tag{4}$$

where H.c. denotes Hermitian conjugate. To arrive at the above expression, we have calculated the functional derivative of the Green's function by adding the local potential variation $\delta U(r) = \delta U_a \delta(r - r_a)$ ($\delta U_a \to 0$) to the Hamiltonian of our system, which leads us to the relation[5]

$$\frac{\delta G(r_n, r_m)}{\delta U(r)} = G(r_n, r) G(r, r_m).$$

Once we have calculated the local PDOS, we can obtain the global PDOS by adding the local PDOS over the particles of our system:

$$\frac{dN_{nm}}{dE} = \sum_k \frac{dn_{nm}(r_k)}{dE}. \tag{5}$$

After summation over the indices i, j, and r_k, the above equation can be presented in matrix form:

$$\frac{dN_{nm}}{dE} = -\frac{\hbar\sqrt{v_n v_m}}{4\pi}(s_{mn}^* Q_{nm} + \mathrm{H.c.}), \tag{6}$$

where the Q_{nm} matrix is defined as

$$Q_{mn} = \tilde{\chi}_n \left(\sum_{j=1}^{M} G_{mj} G_{jn} \right) \tilde{\chi}_m^T \tag{7}$$

and $\tilde{\chi}_n$ is the column matrix:

$$\tilde{\chi} = \begin{pmatrix} \chi_n(1) \\ \vdots \\ \chi_n(M) \end{pmatrix}. \tag{8}$$

Here, $\tilde{\chi}_m^T$ is the transpose of column matrix $\tilde{\chi}_m$ and G_{mj} is the matrix of $M \times M$ rank (M is the number of modes in each lead, see the Appendix).

Finally, $\nu_{\alpha\alpha}$ and $\nu_{\alpha\beta}$ can be obtained from global PDOS dN_{nm}/dE by summing every mode n in lead α and every mode m in lead β, respectively:

$$\nu_{\alpha\alpha} = \sum_{n,m\in\alpha} \frac{dN_{nm}}{dE}, \tag{9}$$

$$\nu_{\alpha\beta} = \sum_{n\in\alpha,m\in\beta} \frac{dN_{nm}}{dE}. \tag{10}$$

$\nu_{\beta\beta}$ and $\nu_{\beta\alpha}$ can be written similarly. Thus, the global DOS ν must be the sum of all global PDOS:

$$\nu = \nu_{\beta\beta} + \nu_{\alpha\alpha} + \nu_{\alpha\beta} + \nu_{\beta\alpha}. \tag{11}$$

In the case of a Q1D wire with the set of δ potentials [see Eq. (1)] in all the quantities in Eqs. (5), (9), and (10), calculated for the tight-binding model, one must replace the summation sign by the appropriate spatial integration.

The paper is organized as follows: In Sec. II, we present our model and the relevant assumptions for the numerical calculations to obtain the probability distributions of $\nu_{\alpha\alpha}$ and $\nu_{\alpha\beta}$ for different regimes. In Sec. III, we study the behavior of var($\nu_{\alpha\alpha}$) and var($\nu_{\alpha\beta}$) as a function of disorder strength w. In Sec. IV, we calculate the distribution functions for $\nu_{\alpha\alpha}$ and $\nu_{\alpha\beta}$ in three different regimes of transport mentioned in Sec. I. The conclusions of the paper are presented in Sec. V.

II. THE MODEL AND NUMERICAL PROCEDURES

For the numerical study, we consider a quasi-one-dimensional lattice of size $L\times W$ ($L\gg W$), where L is the length and W is the width of the system. The standard tight-binding Hamiltonian with nearest-neighbor interaction is

$$H = \sum_i \epsilon_i |r_i\rangle\langle r_i| - t\sum_{i,j} |r_i\rangle\langle r_j|, \tag{12}$$

where ϵ_i is the energy of site i chosen randomly between $\left(-\frac{w}{2},\frac{w}{2}\right)$ with uniform probability. The double sum runs over nearest neighbors. The hopping matrix element t is taken to be 1, which sets the energy scale, and the lattice constant equals 1, setting the length scale. The energies are measured with respect to the center of the band, so we will always deal with propagating modes. Finally, our sample is connected to two semi-infinite, multimode leads to the left (lead α) and to the right (lead β). The leads are represented by the same Hamiltonian as the system, Eq. (12), but without diagonal disorder. We use hard wall boundary conditions in the direction perpendicular to the leads. For simplicity, we take the number of modes in the left and right leads to be the same (M) and the width of this system W thus equals M (for a tight-binding model, the number of modes coincides with the number of sites in the transverse direction). The conductance of a finite size sample depends on the properties of the system and also on the leads, which must be taken into account appropriately. In order to take the interaction of the conductor with the leads into account, we introduce a self-energy term A as an effective Hamiltonian, which will be calculated as (see, e.g., Ref. 20)

$$A_p(r_{0_i}, r_{0_j}) = -t\sum_{m\epsilon p} \chi_m(r_{0_i}) e^{ik_m a} \chi_m(r_{0_j}), \tag{13}$$

$$A_q(r_{0_l}, r_{0_k}) = -t\sum_{n\epsilon q} \chi_n(r_{0_l}) e^{ik_n a} \chi_n(r_{0_k}), \tag{14}$$

$$A = A_p + A_q. \tag{15}$$

Finally, to allow for the numerical calculation of DF of var($\nu_{\alpha\alpha}$) and var($\nu_{\alpha\beta}$) for $M\gg 1$ and for higher dimensions of the system, we calculate the Green's function as

$$G = (E\hat{I} - \hat{H} - \hat{A})^{-1}. \tag{16}$$

To perform the numerical calculation of the elements of this Green's matrix, we will use Dyson's equation, as in Refs. 22 and 23, propagating strip by strip. This drastically reduces the computational time, because instead of inverting an $L^2\times M^2$ matrix, we just have to invert $L\times M$ matrices L times. In this way, we build up the complete lattice starting from a single strip and introduce one by one the interaction with the next strip. Each time we introduce a new strip, we apply the recursion relations of Dyson's equation, until we finally obtain the Green's function for the complete lattice. Once we have determined the Green's function matrix, we calculate var($\nu_{\alpha\alpha}$) and var($\nu_{\alpha\beta}$) according to Eqs. (9) and (10) and obtain their probability distributions for random potentials. Over 250 000 independent impurity configurations were averaged for each N. Finally, the localization length ξ is obtained from the decay of the average of the logarithm of the conductance, $\ln g$, as a function of the system size L,

$$\xi^{-1} = -\lim_{L\to\infty} \frac{1}{2L}\langle \ln g\rangle, \tag{17}$$

where g is given by the Büttiker-Landauer formula[20,24]

$$g = \frac{2e^2}{h}\sum_{n,m} T_{nm}. \tag{18}$$

T_{nm} is the transmission coefficient from mode n to mode m and is calculated in the Appendix for the two mentioned models.

III. var($\nu_{\alpha\alpha}$) AND var($\nu_{\alpha\beta}$) VERSUS w

In this section, we will study the dependence of the var($\nu_{\alpha\alpha}$) and var($\nu_{\alpha\beta}$) vs disorder w and vs the number of mode M. In Fig. 1, we show the behavior of var($\nu_{\alpha\alpha}$) and var($\nu_{\alpha\beta}$) as a function of disorder w, which is plotted for a sample of L=400 and M=4. The crossover defines a critical value of disorder w_c. In Fig. 2, we show the dependence of the critical value w_c on the number of modes M for several samples. The crossing point moves to the left and the w_c decreases with increasing numbers of modes. This means that in the weak localized regime, in analogy with 1D systems, the ratio of localization length ξ to the longitudinal size of the sample L for given modes M follows, in a good approximation, the relationship

$$\frac{\xi}{L} \simeq C(M, w_c, E), \tag{19}$$

where C is a constant that depends on M, w_c, and energy. Equation (19) can be also written in the form

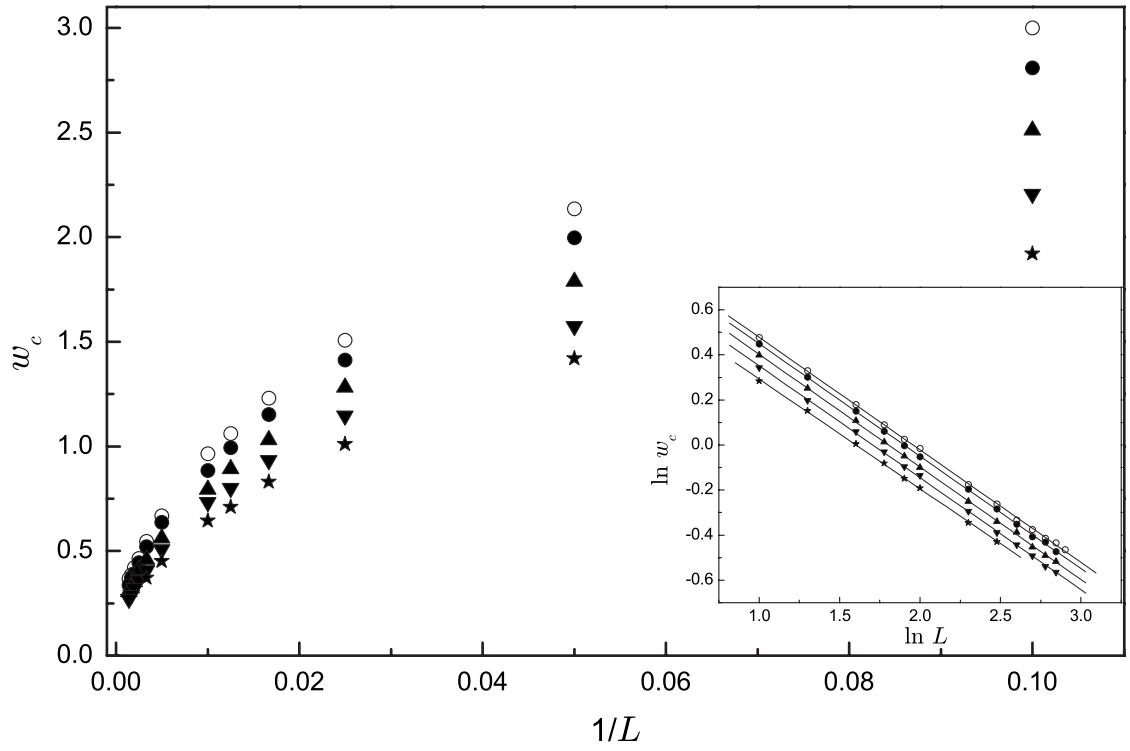

FIG. 2. Critical value w_c for several samples as a function of $1/L$: ○ is for 1D sample; ●, ▲, ▼, and ∗ are for Q1D samples with the number of modes $M=2$, 3, 4, and 5, respectively. The inset presents dependence $\ln w_c$ vs $\ln L$. The slope of the straight line is −0.5 and shows that $L \propto 1/w_c^2$.

$$\xi \simeq M w_c^{-2}, \tag{20}$$

which indicates that in the weak disorder regime, the localization length for a Q1D conductor with large number of transversal channels M, is proportional to w_c^{-2} or to the mean free path.[25] The inset of Fig. 2, where we plot $\ln w_c$ vs $\ln L$, shows that the curves in Fig. 2 are fitted well by straight lines and that the slopes of the straight lines are −0.5, in agreement with Eq. (20).

Note that with the appropriate choice of an effective length $L_{eff}=L(a+bM^c)$ (with $a=0.967$, $b=0.035$, and $c=2.33$), we were able to show that all the curves presented in Fig. 2 collapse into one universal curve in the Q1D system, supporting the hypothesis of single-parameter scaling[26] in disordered systems. In Fig. 3, we plot this universal curve for w_c as a function of $1/L_{eff}$. The different values for the modes are specified inside the figure.

Let us finally remark that in a strictly 1D system, following Ref. 5, one can write ($\nu_T \equiv \nu_{\alpha\beta}+\nu_{\beta\alpha}$ and $\nu_R \equiv \nu_{\alpha\alpha}+\nu_{\beta\beta}$)

$$\langle \ln \nu_R \rangle = \langle \ln \nu \rangle + \langle \ln R \rangle, \tag{21}$$

$$\langle \ln \nu_T \rangle = \langle \ln \nu \rangle + \langle \ln T \rangle, \tag{22}$$

where ν is the global DOS and is defined by Eq. (11). R and T are the reflection and transmission coefficients, respectively and $\langle \cdots \rangle$ denotes averaging over the ensemble. Using the asymptotic behavior of $\langle \ln T \rangle$ and $\langle \ln R \rangle$ as $L \to \infty$ (see, e.g., Ref. 27), these expressions in the weak disorder regime can be written as

$$\langle \ln \nu_R \rangle = \langle \ln \nu \rangle + \ln(1 - e^{-2L/\xi}), \tag{23}$$

$$\langle \ln \nu_T \rangle = \langle \ln \nu \rangle - 2L/\xi, \tag{24}$$

where an average over the ensemble $\ln \nu$ can be numerically calculated directly from Eq. (11). In Fig. 4, we plot the average of $\ln \nu_R$ and $\ln \nu_T$ for different values of disorder w_c as a function of L/ξ. We see that the numerical data for these

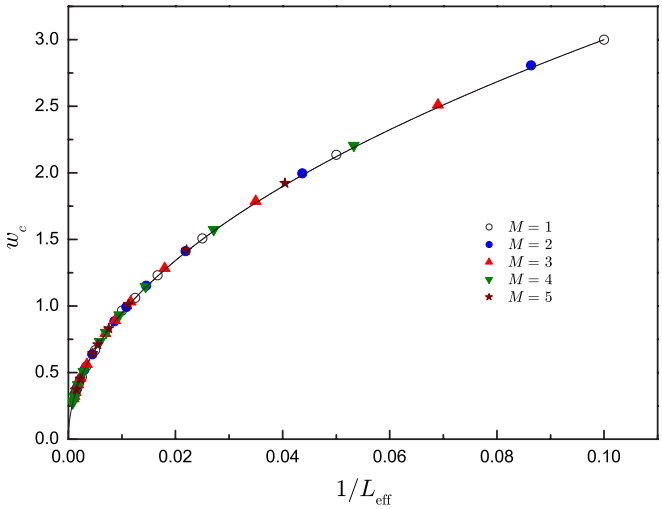

FIG. 3. (Color online) Universal curve w_c for several samples as a function of $1/L_{eff}$. ○ is for 1D sample; ●, ▲, ▼, and ∗ are for Q1D samples with the number of modes $M=2$, 3, 4, and 5, respectively.

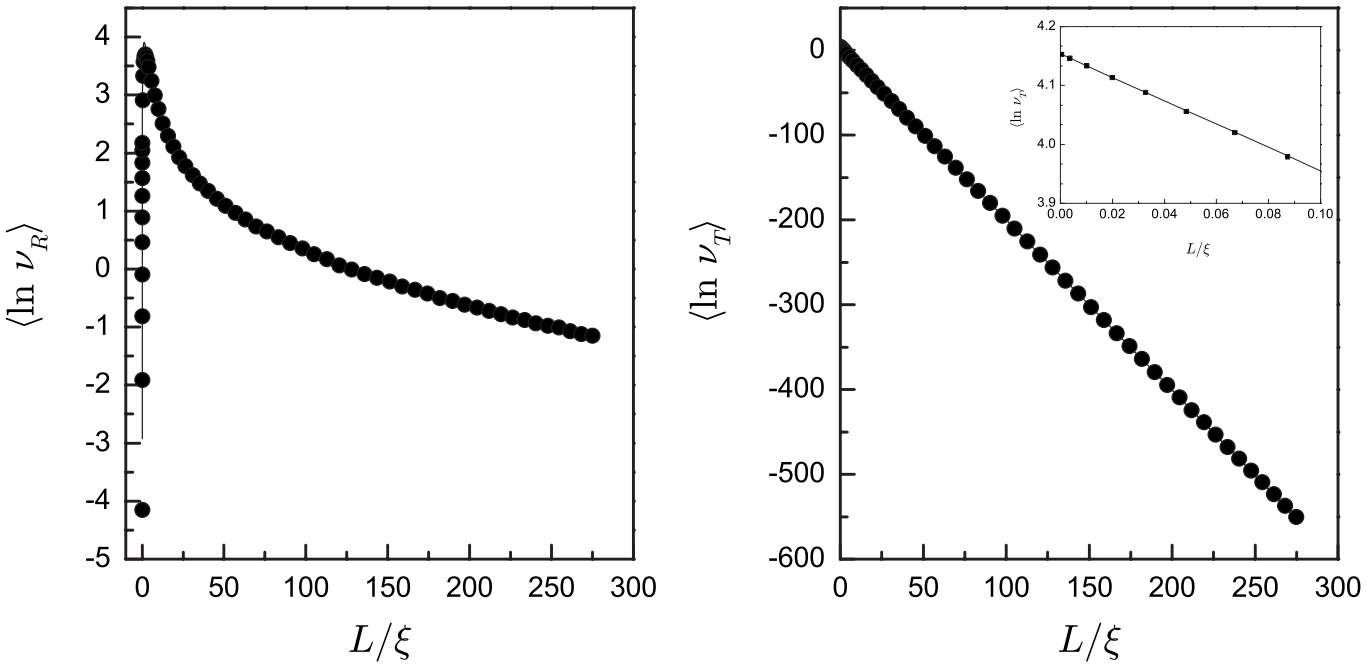

FIG. 4. Average of ln ν_R and ln ν_T as a function of L/ξ. Solid curves are given by Eqs. (23) and (24). The data points (●) are the numerical results for a sample of $L=400$. The inset shows an enlargement of the region near $L/\xi=0$, in the same units.

quantities coincide with Eqs. (23) and (24) for small w_c or for large L/ξ. For the sake of clarity, we have shown an enlargement of the region near $L/\xi=0$ in the inset of Fig. 4.

IV. PLOTS AND DISCUSSION

In this section, we analyze the DF $P(\nu_{\alpha\alpha})$ and $P(\nu_{\alpha\beta})$ along the transition from the metallic to the insulating regime for several sample sizes and for the two models mentioned in Sec. I. We found that the relative shape of the DF depends only on the disorder parameter L/ξ, i.e., when we increase the number of modes M we can always find an appropriate range of w for which all the curves have the same form. Therefore, in the remainder of this section, we present our results for a sample of $L=400$ and $M=4$ for several values of disorder w without loss of generality.

The distribution functions in the metallic regime, when the system size is much smaller than the localization length, $L \ll \xi$, are shown in Fig. 5, with $W=0.2$, $L/\xi=0.17$, and $\langle g \rangle = 2.52$. We have checked that the distribution $P(\nu_{\alpha\beta})$ is Gaussian-like and can be fitted with the following expression ($B=1.0$, $\mu=116.5$, and $\sigma=20.2$):

$$P(\nu_{\alpha\beta}) = \frac{B}{\sqrt{2\pi}\sigma} e^{-(\nu_{\alpha\beta}-\mu)^2/2\sigma^2}. \tag{25}$$

Although we deal with Q1D systems in our numerical studies (the number of modes $M>1$), the Gaussian-like behavior of the $\nu_{\alpha\beta}$ in the ballistic regime can be understood well if we recall the fact that $\nu_{\alpha\beta}$ is connected with physically meaningful times characterizing the tunneling process.[5] Indeed, according to Ref. 5, in 1D systems, global PDOS is related to the Larmor transmitted time τ_T (or Wigner delay time) weighted by the transmission coefficient:

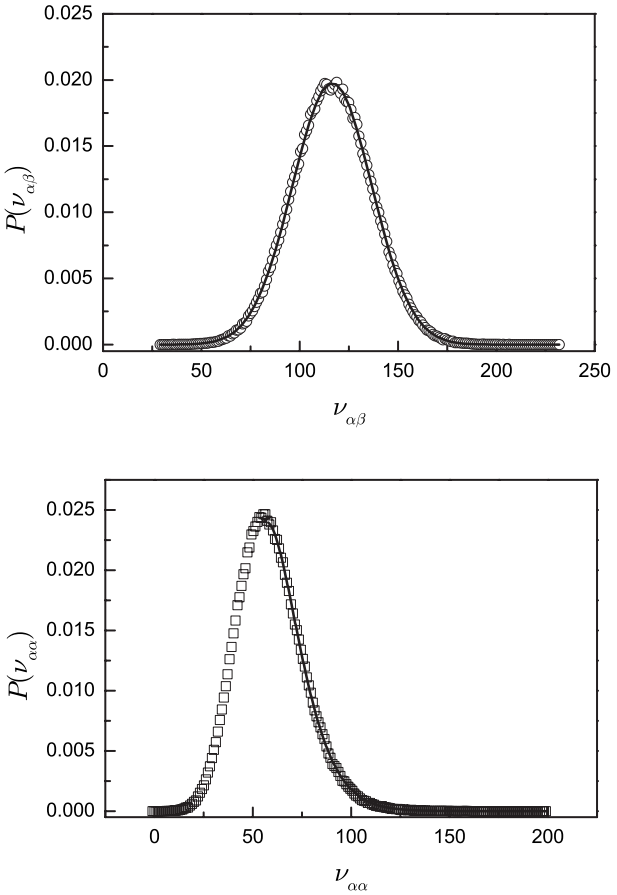

FIG. 5. Probability distributions of $\nu_{\alpha\alpha}$ and $\nu_{\alpha\beta}$ in the metallic regime ($\langle g \rangle = 2.52$) for a disorder of $w=0.2$. The solid lines correspond to a Gaussian distribution for $\nu_{\alpha\beta}$ and a log-normal tail distribution for $\nu_{\alpha\alpha}$.

$$\nu_{\alpha\beta} = \frac{T}{2}\tau_T, \tag{26}$$

where the quantity τ_T is related to the DOS of the system,[28]

$$\tau_T = \hbar \,\mathrm{Im}\int_0^L G(x,x)dx = \hbar \,\mathrm{Im}\left(\frac{\partial \ln t}{\partial E} + \frac{r+r'}{4E}\right). \tag{27}$$

Here, $G(x,x)$ is the Green's function for the whole system, and t and r are the transmission and reflection amplitudes for the finite system. r' is the reflection amplitude of the electron for the whole system, when it is incident from the right. The second term in Eq. (27) becomes important at low energies and/or short systems. This term can be neglected in the semiclassical WKB case and, of course, when r (and thus r') is negligible, e.g., in the resonant case, when the influence of the boundaries is negligible.

As one can see from Eq. (26), the distribution function of $\nu_{\alpha\beta}$ is affected by correlations between the value of the DOS (or Wigner delay time) and the transmission coefficient of resonances via localized states, but it still captures the general behavior of the Wigner delay time in 1D systems in the regime $T \sim 1$. As was pointed out in Refs. 29 and 30, basing on the invariant embedding method, the DF of the Wigner delay time for ballistic systems is universal, given by a Gaussian function, and can be characterized by a first moment and a second cumulant. A similar result for delay-time distribution was also predicted in Ref. 31, using random-matrix theory. In other words, if the system is very transmissive, then the inductivelike dynamic behavior dominates. Note that the DF of transmission delay time for single-channel waveguide for all τ_T is analytically calculated in Ref. 13.

A relation similar to Eq. (26) holds for $\nu_{\alpha\alpha}$:

$$\nu_{\alpha\alpha} = \frac{R}{2}\tau_R, \tag{28}$$

where τ_R is the reflection time defined as

$$\tau_R = \hbar \,\mathrm{Im}\,\frac{1+r}{r}e^{-i2\theta(0)}\int_0^L G(x,x)e^{i2\theta(x)}dx$$
$$= \hbar \,\mathrm{Im}\left(\frac{\partial \ln r}{\partial E} - \frac{1-r^2-t^2}{4Er}\right), \tag{29}$$

with

$$\theta(x) = \exp\left[\int_0^x \frac{dx}{2G(x,x)}\right].$$

We note that for an arbitrary symmetric potential, $V[(L/2)+x]=V[(L/2)-x]$, the total phases accumulated in a transmission and in a reflection event are the same and thus the characteristic times for transmission and reflection corresponding to the direction of propagation are equal,

$$\tau_T = \tau_R, \tag{30}$$

as follows from Eqs. (27) and (29). For the special case of a rectangular barrier, Eq. (30) was first found in Ref. 32. Comparison of Eqs. (27) and (29) shows that for an asymmetric barrier, Eq. (30) breaks down.[33]

One can see from Fig. 5 that the DF $P(\nu_{\alpha\alpha})$ in the same regime includes a big range of negative $\nu_{\alpha\alpha}$ values, indicating a predominantly inductive dynamic response of the system to an external ac electric field.[16] To try to get more hints on the form of the DF for positive values of $\nu_{\alpha\alpha}$, we have calculated higher order cumulants as a function of the L. It turns out that for positive values of $\nu_{\alpha\alpha}$ the tail of the distribution $P(\nu_{\alpha\alpha})$ is fairly log-normal with the parameters $B=0.875$, $\mu=60.5$, and $\sigma=0.25$.

$$P(\nu_{\alpha\alpha}) = \frac{B}{\sqrt{2\pi}\sigma\nu_{\alpha\alpha}}e^{-(\ln \nu_{\alpha\alpha}-\mu)^2/2\sigma^2}. \tag{31}$$

With increase of disorder w, when we are almost in the crossover regime, we obtain a wide range of broad distributions, as shown in Fig. 6. Here, we plot DF for two values of disorder: $w=0.5$ ($L/\xi=0.69$ and $\langle g\rangle=0.75$) in the left panel and $w=0.6$ ($L/\xi=0.93$ and $\langle g\rangle=0.5$) in the right panel. As one can see from Fig. 6 (right panel), $P(\nu_{\alpha\beta})$ has a constant region for almost the full range of $\nu_{\alpha\beta}$, while in the left panel, it decreases rapidly. In both cases, the distributions for $P(\nu_{\alpha\beta})$ can be fitted to two log-normal tails. This type of behavior is typical for distributions of conductance g in the same range of parameters in Q1D, as one can see from the same figure where we present $P(g)$. For values $g<1$, we have a flat part, while in the regime $g>1$, the distribution of conductance decreases rapidly. This is in complete agreement with a number of numerical simulations in the intermediate regime (see, e.g., Refs. 34–36).

$P(\nu_{\alpha\alpha})$ is shifted to the right in Fig. 6, to much larger values of $\nu_{\alpha\alpha}$, which means that it becomes less conductive. For this range of parameters, DF is still quite symmetric (right panel) but broader if we compare it with the DF from Fig. 5. The $P(\nu_{\alpha\alpha})$ for $w=0.6$ becomes less symmetric (left panel).

With further increase of disorder w (in the insulating region), $P(\nu_{\alpha\beta})$ becomes a one-sided log-normal distribution. This type of behavior was predicted for distributions of conductance g (Refs. 36 and 37) and numerically calculated.[34,35,38]

With regard to $P(\nu_{\alpha\alpha})$, we can mention that the tail of the distribution follows a power-law decay $P(\nu_{\alpha\alpha}) \propto 1/\nu_{\alpha\alpha}^m$, with $m \simeq 2.3$. The power-law decay tail for delay time in the localized regime as also found in Refs. 13, 29, and 39. On the other hand, as w increases, $P(\nu_{\alpha\beta})$ shows a tail in the negative region of $\nu_{\alpha\beta}$. In Fig. 7, we plot the distributions $P(\nu_{\alpha\alpha})$ and $P(\nu_{\alpha\beta})$ for disorder $w=1$ ($L/\xi=2.6$ and $\langle g\rangle=0.08$).

Deeply in the localized regime ($L \gg \xi$ and $\langle g\rangle \approx 0$), the distribution of $\nu_{\alpha\beta}$ is log-normal, as one can see from Fig. 8, where we fitted $P(\ln \nu_{\alpha\beta})$ to a Gaussian distribution:

$$P(x) = \frac{B}{\sqrt{2\pi}\sigma x}e^{-(\ln x-\mu)^2/2\sigma^2}, \tag{32}$$

with $B=0.997$, $\mu=-460.5$, and $\sigma=27.7$.

The shape of $P(\nu_{\alpha\alpha})$ is highly asymmetric with two peaks very close to each other. The position and the amplitude of

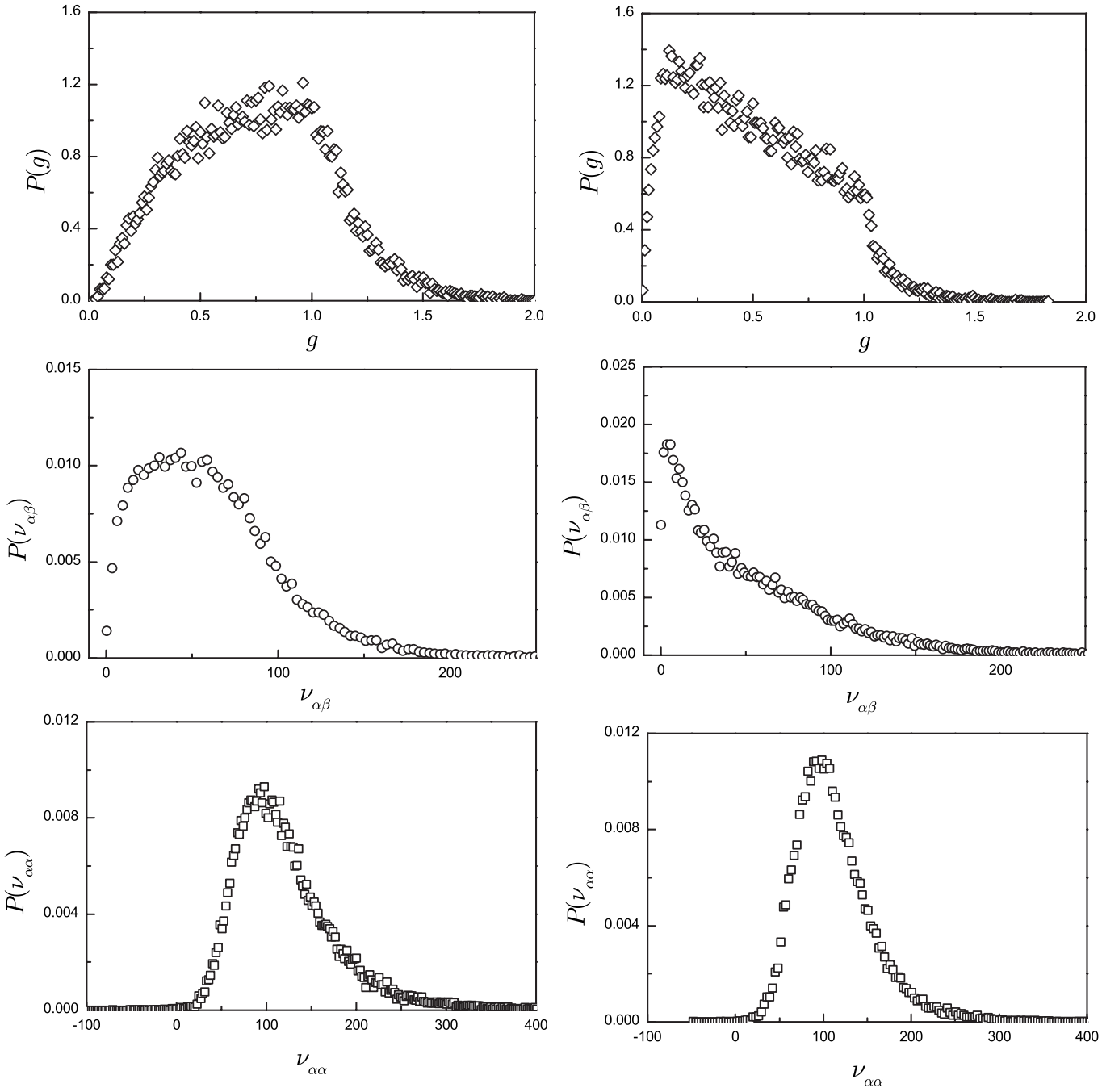

FIG. 6. Distributions $P(g)$, $P(\nu_{\alpha\alpha})$, and $P(\nu_{\alpha\beta})$ in the crossover regime for two values of the disorder: right panel for $w=0.5$ ($L/\xi=0.69$ and $\langle g\rangle=0.75$) and left panel for $w=0.6$ ($L/\xi=0.93$ and $\langle g\rangle=0.5$).

these peaks depend on the disorder parameter and cause several fluctuations in the distribution function. The tail of the distribution follows a power-law decay $P(\nu_{\alpha\alpha}) \propto 1/\nu_{\alpha\alpha}^{m}$, with $m \simeq 2.0$.

V. CONCLUSIONS

We have studied the distribution functions for the global partial density of states in quasi-one-dimensional disordered wires as a function of disorder parameter from metal to insulator. We consider two different models for a disordered Q1D wire: a set of two-dimensional δ potentials with signs and strengths determined randomly and a tight-binding Hamiltonian with several modes and on-site disorder. It was shown that the poles of the Green's functions for these models can be presented, as was done in the 1D case,[42] as a determinant of rank $N\times N$ (N is the number of scatterers), where the matrix elements depend on the model, type of disorder, and number of modes, M. The determinant can be used to calculate the spectrum of an electron in the disordered Q1D wire, the DOS, the scattering matrix elements, etc., without determining the exact electron wave function.

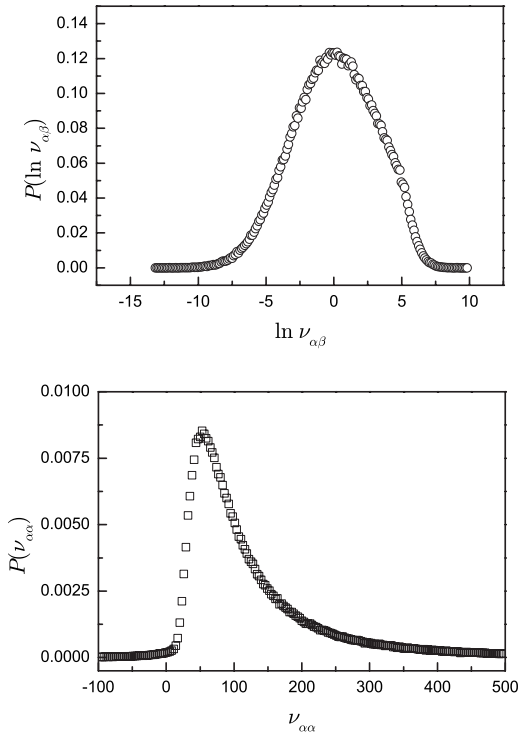

FIG. 7. Distributions $P(\nu_{\alpha\alpha})$ and $P(\ln \nu_{\alpha\beta})$ in the insulating regime ($\langle g\rangle=0.08$) for a disorder of $w=1$. We have a one-sided log-normal distribution for $\nu_{\alpha\beta}$ and power-law tail for $\nu_{\alpha\alpha}$, $P(\nu_{\alpha\alpha}) \propto 1/\nu_{\alpha\alpha}^{m}$, with $m \simeq 2.3$.

We show that the variances of partial global DOS in the metal to insulator crossover regime are crossing. We also show that with increase of the number of modes, M, the crossing point moves to the left, i.e., w_c decreases. The critical value of disorder w_c, where crossover occurs, can be used to calculate localization length in Q1D systems.

In the metallic regime, when the system size is much smaller than the localization length, $L \ll \xi$, the DF for $P(\nu_{\alpha\beta})$ is Gaussian-like. In the same regime, the distribution function $P(\nu_{\alpha\alpha})$ includes a large range of negative $\nu_{\alpha\alpha}$ values, indicating a predominantly inductive dynamic response of the system to an external ac electric field.[16] For positive values of $\nu_{\alpha\alpha}$, the tail of the distribution $P(\nu_{\alpha\alpha})$ is fairly log-normal. In the vicinity of the crossover regime, the distribution function for $P(\nu_{\alpha\beta})$ can be fitted to two log-normal tails. $P(\nu_{\alpha\alpha})$ is shifted to the right, to much larger values of $\nu_{\alpha\alpha}$, which means that it becomes less conductive. Further increase of disorder w (in the insulating region) affects the $P(\nu_{\alpha\beta})$ and it becomes a one-sided log-normal distribution. With regard to $P(\nu_{\alpha\alpha})$, we can mention that the tail of the distribution follows a power-law decay $P(\nu_{\alpha\alpha}) \propto 1/\nu_{\alpha\alpha}^{m}$, with $m \simeq 2.3$. Deep in the localized regime ($L \gg \xi$ and $\langle g\rangle \approx 0$), the distribution of $\nu_{\alpha\beta}$ is log-normal, while the shape of $P(\nu_{\alpha\alpha})$ is highly asymmetric with two peaks very close to each other. The position and amplitude of these peaks depend on the disorder parameter and cause fluctuations in the distribution function. In general, the system shows inductivelike dynamic behavior when it is almost transparent, and it behaves capacitivelike when we have complete reflection from the system.

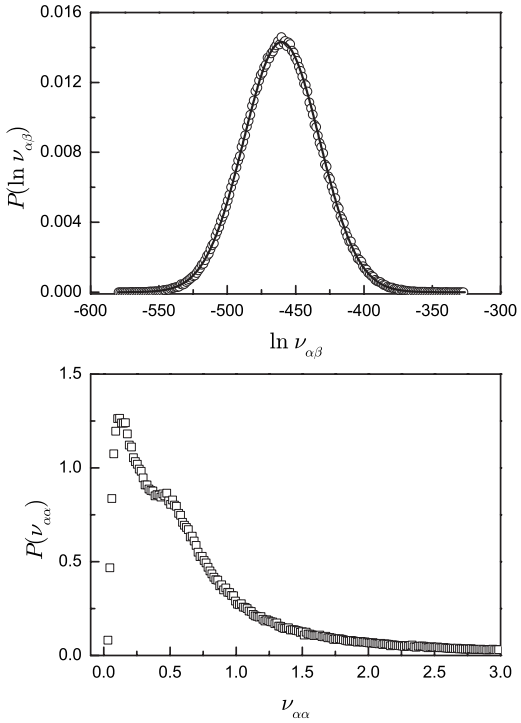

FIG. 8. Distributions $P(\nu_{\alpha\alpha})$ and $P(\ln \nu_{\alpha\beta})$ in the insulating regime ($\langle g\rangle \approx 0$) for a disorder of $w=12$. The solid lines correspond to a Gaussian distribution for $\ln \nu_{\alpha\beta}$ that exhibit a log-normal distribution for $\nu_{\alpha\beta}$. The tail of the distribution follows a power-law decay $P(\nu_{\alpha\alpha}) \propto 1/\nu_{\alpha\alpha}^{m}$, with $m \simeq 2.0$.

ACKNOWLEDGMENTS

One of the authors (V.G.) thanks M. Büttiker and T. Meyer for useful discussions and acknowledges the kind hospitality extended to him at Murcia and Geneva Universities. Another author (J.R.) thanks the FEDER and the Spanish DGI for financial support through Project No. FIS2004-03117.

APPENDIX: DYSON EQUATION IN A Q1D DISORDERED SYSTEM AND THE POLES OF GREEN'S FUNCTION

Our main result in this appendix shows that we can express the reflection and transmission amplitudes from mode n to mode m, R_{nm} and T_{nm}, for the potential $V(x)$, Eq. (1), from its characteristic determinants without knowledge of the exact electron wave functions. This means that the Q1D problem can be mapped to the 1D problem and that the poles of the Green's function matrix elements, as well as the scattering matrix elements T_{nm} and R_{nm}, conductance [Eq. (18)], etc., are a determinant of rank $N \times N$, where N is the number of scatterers.

Let us write down once more the impurity potential:

$$V(x,y) = \sum_{n=1}^{N} V_n \delta(x - x_n)\,\delta(y - y_n), \tag{A1}$$

where V_n, x_n, and y_n are arbitrary parameters.

The equation for the GF with the above potential $V(x,y)$ is

$$\left\{E-\left[-\frac{\hbar^2}{2m}\left(\frac{d^2}{dx^2}+\frac{d^2}{dy^2}\right)+V_c(y)+V(x,y)\right]\right\}G(xy;x'y') = \delta(x-x')\delta(y-y'), \tag{A2}$$

where the confinement potential $V_c(y)$ depends only on the transverse direction y. The Dyson equation for a Q1D wire can be written in the form[40]

$$G_{ac}(x,x') = G_a^0(x,x')\delta_{ac} + \sum_{b,d}\int G_a^0(x,x'')\delta_{ab}V_{bd}(x'')G_{dc}(x'',x')dx''. \tag{A3}$$

The matrix $V_{ab}(x)$ elements of the defect potential are

$$V_{ab}(x) = \int \chi_a^*(y)V(x,y)\chi_b(y)dy = \sum_{n=1}^{N} V_{ab}^{(n)}\delta(x-x_n), \tag{A4}$$

with $V_{ab}^{(n)}$ defined as

$$V_{ab}^{(n)}(x) = \chi_a^*(y_n)V_n\chi_b(y_n). \tag{A5}$$

Details of the calculation of the matrix elements of GF $G_{nm}(x,x')$ of the Dyson equation [Eq. (A3)] for this case, based on the method developed in Refs. 41 and 42, will be given elsewhere.[19] Here, we only present the basic output of the calculation of the Dyson equation, which shows that the pole of GF can be rewritten as a determinant of rank $MN \times MN$ (M is the number of modes and N is the number of δ potentials).

The matrix elements of determinant

$$D_{MN} = \frac{\det D_{n,l}^{(MN)}}{\prod_{l=1}^{N}\left[1+\sum_{p=1}^{M} r_{pp}^{(l)}\right]} \tag{A6}$$

are

$$D_{n,l}^{(MN)} = -I\delta_{nl} + (I-\delta_{nl})\{\lambda_{nl}\}\{r^{(l)}\}, \quad 1 \leqslant n,l \leqslant N, \tag{A7}$$

where

$$I = \begin{pmatrix} 1 & \cdots & 0 \\ \vdots & \ddots & \vdots \\ 0 & \cdots & 1 \end{pmatrix} \tag{A8}$$

is the unit matrix. The lth scattering matrix $\{r^{(l)}\}$ and the $\{\lambda_{nl}\}$ matrix are matrices of rank $M \times M$, defined in the following way:

$$\{r^{(l)}\} = \begin{pmatrix} r_{11}^{(l)} & \cdots & r_{1M}^{(l)} \\ \vdots & \ddots & \vdots \\ r_{M1}^{(l)} & \cdots & r_{MM}^{(l)} \end{pmatrix}, \tag{A9}$$

$$\{\lambda_{nl}\} = \begin{pmatrix} \lambda_{nl}^{(1)} & \cdots & 0 \\ \vdots & \ddots & \vdots \\ 0 & \cdots & \lambda_{nl}^{(M)} \end{pmatrix} = \begin{pmatrix} e^{ik_1|x_n-x_l|} & \cdots & 0 \\ \vdots & \ddots & \vdots \\ 0 & \cdots & e^{ik_M|x_n-x_l|} \end{pmatrix}. \tag{A10}$$

The quantity $r_{km}^{(l)}$,

$$r_{km}^{(l)} = \frac{V_{km}^{(l)}\sqrt{G_k^0(x_l,x_l)G_m^0(x_l,x_l)}}{1-\sum_{p=1}^{M} V_{pp}^{(l)}G_p^0(x_l,x_l)}, \tag{A11}$$

is the complex reflection amplitude of an electron from the isolated potential V_l with the coordinates x_l, y_l. Electrons are incident from the normal mode m $(m=1,2,\ldots,M)$ on the left (right) side and reflected from the normal mode k on the same side. By permuting indices k and m in Eq. (A11), one can find the complex amplitude $r_{mk}^{(l)}$. Note that the determinant of the matrix $r^{(l)}$ is zero, i.e.,

$$\det\{r^{(l)}\} = 0. \tag{A12}$$

This follows from the fact that

$$r_{mm}^{(l)}r_{kk}^{(l)} - r_{mk}^{(l)}r_{km}^{(l)} = 0,$$

which can be checked directly if one uses the definition of $r_{km}^{(l)}$ [see Eq. (A11)].

The rank $MN \times MN$ of the above determinant [see Eq. (A7)], after some mathematical manipulation, can be reduced to the determinant of rank $N \times N$, as in the case of a 1D chain of arbitrarily arranged potentials,[41,42] with the following matrix elements, which now contain information about the number of modes M:

$$D_{n,l}^{(N)} = -\delta_{nl} + (1-\delta_{nl})\sum_{p=1}^{M}\frac{r_{1p}^{(n)}r_{p1}^{(l)}\lambda_{nl}^{(p)}}{r_{11}^{(n)}}, \quad 1 \leqslant n,l \leqslant N. \tag{A13}$$

Once we know the explicit form of determinant D_N,

$$D_N = \frac{(-1)^N \det D_{n,l}^{(N)}}{\prod_{l=1}^{N}\left[1+\sum_{p=1}^{M} r_{pp}^{(l)}\right]}, \tag{A14}$$

i.e., the poles of GF, we can calculate the spectrum of an electron in the disordered Q1D wire, the DOS, the scattering matrix elements, etc., without determining the exact electron wave function in the disordered Q1D wire. The form of the determinant is valid for δ-function potentials of arbitrary strength and for arbitrary number of propagating and evanescent modes M. Note that Eq. (A13) reduces to a characteristic determinant (see Refs. 41 and 42) if there is no coupling to the second, third, etc., modes, i.e., $r_{p1}^{(p)}=0$.

This is our main result. In the following, we will show how to calculate the scattering matrix $T_{nm}^{(N)}$ and $R_{nm}^{(N)}$ elements and the electronic spectra of the Q1D disordered wire.

The transmission amplitude $T_{nm}^{(N)}$ $(n \geqslant m)$ from the set of $N\delta$ potentials can be presented:

$$T_{nm}^{(N)} = e^{ik_1|x_N - x_1|} \frac{\det \tilde{D}_{n,l}^{(N)}}{\det D_{n,l}^{(N)}}, \tag{A15}$$

where the matrix $\tilde{D}_{n,l}^{(N)}$ is obtained from the matrix $D_{nl}^{(N)}$ [Eq. (A13)] by augmenting it on the left and on the top in the following way:

$$\tilde{D}_{n,l}^{(N)} = \begin{vmatrix} 1 & r_{nm}^{(l)} & \cdots & r_{nm}^{(N)} e^{ik_1|x_N - x_1|} \\ 1 & \cdots & \cdots & \cdots \\ \vdots & \vdots & D_{n,l}^{(N)} & \\ e^{-ik_1|x_N - x_1|} & \vdots & & \end{vmatrix}. \tag{A16}$$

The reflection amplitude $R_{nm}^{(N)}$ $(n \geqslant m)$ of electrons from the same set of N δ potentials is given by

$$R_{nm}^{(N)} = \frac{\det \bar{D}_{nl}^{(N)}}{\det D_{nl}^{(N)}}, \tag{A17}$$

where the matrix $\bar{D}_{nl}^{(N)}$ is obtained from the matrix $D_{nl}^{(N)}$ [Eq. (A13)] by augmenting it on the left and on the top:

$$\bar{D}_{n,l}^{(N)} = \begin{vmatrix} 0 & r_{nm}^{(l)} & \cdots & r_{nm}^{(N)} e^{ik_1|x_N - x_1|} \\ 1 & \cdots & \cdots & \cdots \\ \vdots & \vdots & D_{n,l}^{(N)} & \\ e^{ik_1|x_N - x_1|} & \vdots & & \end{vmatrix}. \tag{A18}$$

It can be checked directly that Eq. (A15), for the case of two point scatterers (i.e., $N=2$) and for two modes ($M=2$) when $n=m=1$, leads us to ($a_1 = x_2 - x_1$)

$$T_{11}^{(2)} = e^{ik_1 a_1} \frac{[1 + r_{11}^{(1)}][1 + r_{11}^{(2)}] + r_{12}^{(1)} r_{21}^{(2)} e^{i(k_2 - k_1)a_1} - r_{22}^{(1)} r_{22}^{(2)} e^{2ik_2 a_1} - e^{i(k_1 + k_2)a_1} r_{12}^{(2)} r_{21}^{(1)}}{1 - r_{11}^{(1)} r_{11}^{(2)} e^{2ik_1 a_1} - r_{22}^{(1)} r_{22}^{(2)} e^{2ik_2 a_1} - [r_{12}^{(1)} r_{21}^{(2)} + r_{21}^{(1)} r_{12}^{(2)}] e^{i(k_1 + k_2)a_1}},$$

which, after the appropriate notation used in Ref. 43 will coincide with their expression of T_{11} calculated by the transfer matrix method.

For the same case of $N=M=2$, $R_{11}^{(2)}$ is obtained from Eq. (A17),

$$R_{11}^{(2)} = \frac{r_{11}^{(1)} + r_{11}^{(2)}[1 + 2r_{11}^{(1)}] e^{2ik_1 a_1} + [r_{12}^{(1)} r_{21}^{(2)} + r_{21}^{(1)} r_{12}^{(2)}] e^{i(k_1 + k_2)a_1}}{1 - r_{11}^{(1)} r_{11}^{(2)} e^{2ik_1 a_1} - r_{22}^{(1)} r_{22}^{(2)} e^{2ik_2 a_1} - [r_{12}^{(1)} r_{21}^{(2)} + r_{21}^{(1)} r_{12}^{(2)}] e^{i(k_1 + k_2)a_1}}.$$

To calculate the energy spectrum of a Q1D system, one must enclose the system between two infinite potentials to make it a close system and calculate the zeros of the determinant D_N, Eq. (A14). This determinant can be calculated recursively and give us most magnitudes of interest, since it is directly related to the GF of the system.

Finally, we note that the expressions for the pole of the GF [Eq. (A7)] for transmission amplitude $T_{nm}^{(N)}$ and for $R_{nm}^{(N)}$ in the tight-binding model are obtained by replacing the unperturbed GF for normal mode m,

$$G_m^0(x,x') = -i \frac{m_0}{\hbar^2 k_m} \exp(ik_m|x - x'|), \tag{A19}$$

with

$$k_m = + \sqrt{\frac{2m_0(E - E_m)}{\hbar^2}}, \tag{A20}$$

by the appropriate GF for the tight-binding model:[44]

$$G_m^0(l,n) = -\frac{i}{\sqrt{B^2 - (E - \epsilon)^2}} e^{|l-n|\Theta}. \tag{A21}$$

Here $[x \equiv (E - \epsilon)/B]$,

$$\Theta = \ln(x - i\sqrt{1 - x^2}) \tag{A22}$$

and the symbol $\sqrt{1-x^2}$ denotes the positive square roots.

[1] M. Büttiker, J. Phys.: Condens. Matter **5**, 9361 (1993).
[2] M. Büttiker, H. Thomas, and A. Prêtre, Z. Phys. B: Condens. Matter **94**, 133 (1994).
[3] M. Brandbyge and M. Tsukada, Phys. Rev. B **57**, R15088 (1998).
[4] Q. Zheng, J. Wang, and H. Guo, Phys. Rev. B **56**, 12462 (1997).
[5] V. Gasparian, T. Christen, and M. Büttiker, Phys. Rev. A **54**, 4022 (1996).
[6] M. Büttiker, *Lecture Notes in Physics* (Springer, Berlin, 2002).
[7] H. Schomerus, M. Titov, P. W. Brouwer, and C. W. J. Beenakker, Phys. Rev. B **65**, 121101(R) (2002).
[8] M. Büttiker, Pramana, J. Phys. **58**, 241 (2002).
[9] M. Switkes, C. M. Marcus, K. Campman, and A. C. Gossard, Science **283**, 1905 (1999).
[10] P. W. Brouwer, Phys. Rev. B **58**, R10135 (1998).

[11] M. Moskalets and M. Büttiker, Phys. Rev. B **66**, 035306 (2002).
[12] C. J. Bolton-Heaton, C. J. Lambert, V. I. Fal'ko, V. Prigodin, and A. J. Epstein, Phys. Rev. B **60**, 10569 (1999).
[13] H. Schomerus, Phys. Rev. E **64**, 026606 (2001).
[14] A. Z. Genack, P. Sebbah, M. Stoytchev, and B. A. van Tiggelen, Phys. Rev. Lett. **82**, 715 (1999).
[15] B. A. van Tiggelen, P. Sebbah, M. Stoytchev, and A. Z. Genack, Phys. Rev. E **59**, 7166 (1999).
[16] M. Büttiker and T. Christen, in *Theory of Transport Properties of Semiconductor Nanostructures*, edited by E. Schöl (Chapman and Hall, London, 1998).
[17] T. De Jesus, H. Guo, and J. Wang, Phys. Rev. B **62**, 10774 (2000).
[18] P. W. Brouwer, K. M. Frahm, and C. W. J. Beenakker, Phys. Rev. Lett. **78**, 4737 (1997).
[19] The details and results will be presented elsewhere.
[20] S. Datta, *Electronic Transport in Mesoscopic Systems* (Cambridge University Press, Cambridge, 1995).
[21] D. S. Fisher and P. A. Lee, Phys. Rev. B **23**, 6851 (1981).
[22] A. MacKinnon, Z. Phys. B: Condens. Matter **59**, 385 (1985).
[23] J. A. Vergés, Comput. Phys. Commun. **118**, 71 (1999).
[24] R. Landauer, J. Phys.: Condens. Matter **1**, 8099 (1989).
[25] Y. Imry, *Introduction to Mesoscopic Physics* (Oxford University Press, New York, 1997).
[26] E. Abrahams, P. W. Anderson, D. C. Licciardello, and T. V. Ramakrishnan, Phys. Rev. Lett. **42**, 673 (1979).
[27] I. M. Lifshitz, S. A. Gredeskul, and L. A. Pastur, *Introduction to the Theory of Disordered Systems* (Wiley, New York, 1988).
[28] V. Gasparian and M. Pollak, Phys. Rev. B **47**, 2038 (1993).
[29] C. Texier and A. Comtet, Phys. Rev. Lett. **82**, 4220 (1999).
[30] J. Heinrichs, Phys. Rev. B **65**, 075112 (2002).
[31] Y. V. Fyodorov and H. J. Sommers, J. Math. Phys. **38**, 1918 (1997); A. Ossipov and Y. V. Fyodorov, Phys. Rev. B **71**, 125133 (2005).
[32] M. Büttiker, Phys. Rev. B **27**, 6178 (1983).
[33] C. R. Leavens and G. C. Aers, Solid State Commun. **63**, 1101 (1987).
[34] M. Rühländer, P. Markoš, and C. M. Soukoulis, Phys. Rev. B **64**, 193103 (2001).
[35] M. Rühländer and C. M. Soukoulis, Phys. Rev. B **63**, 085103 (2001).
[36] V. A. Gopar, K. A. Muttalib, and P. Wölfle, Phys. Rev. B **66**, 174204 (2002).
[37] K. A. Muttalib and P. Wölfle, Phys. Rev. Lett. **83**, 3013 (1999).
[38] A. García-Martín and J. J. Sáenz, Phys. Rev. Lett. **87**, 116603 (2001).
[39] C. W. J. Beenakker and P. W. Brouwer, Physica E (Amsterdam) **9**, 463 (2001).
[40] P. F. Bagwell, J. Phys.: Condens. Matter **2**, 6179 (1990).
[41] V. M. Gasparian, B. L. Altshuler, A. G. Aronov, and Z. H. Kasamanian, Phys. Lett. A **132**, 201 (1988).
[42] A. G. Aronov, V. Gasparian, and U. Gummich, J. Phys.: Condens. Matter **3**, 3023 (1991).
[43] A. Kumar and P. F. Bagwell, Phys. Rev. B **43**, 9012 (1991).
[44] E. N. Economou, *Green's Functions in Quantum Physics* (Springer-Verlag, Berlin, 1983).